The following chapter contains material adapted in part, with permission, from:

Journal of Physical Chemistry C, 114 (28) 12300–12307, Jun 28 2010

http://pubs.acs.org/articlesonrequest/AOR-2zUgS72Z5YFJiekWnC5S

Chapter 4

Electrical Measurements II: Mercury Contacts

4.1 Introduction

This chapter describes the electrical characteristics of Ge(111) electrodes in contact with mercury metal, forming a Schottky diode. The barrier height is determined from both the current-voltage behavior and the differential capacitance measurements.

4.1.1 Background

After contact between a metal and semiconductor is established, the Fermi-levels of the two phases will be level at thermal equilibrium. For the case of an ideal n-type semiconductor in contact with a higher work function metal, the difference in potential between the metal work function $(q\phi_m)$ and the semiconductor Fermi-level $(E_F = q(\chi + V_n))$ is dropped across the space-charge region. The energy barrier to electron injection from the metal into the semiconductor conduction band is solely determined by the metal work-function and the semiconductor electron affinity.

$$q\phi_{Bn} = q\left(\phi_M - \chi\right) \tag{4.1}$$

Thermionic emission theory relates the barrier height to the diode current-voltage (J-V) behavior as

$$J_n = J_{ST}\left[\exp\left(\frac{qV}{kT}\right) - 1\right] \tag{4.2}$$

$$J_{ST} = A^*T^2\exp\left(\frac{-q\phi_{Bn}}{kT}\right) \tag{4.3}$$

by considering the net carrier flux as the sum of the flow from the semiconductor to the metal and from the metal to the semiconductor. A^* is the Richardson constant. The first term within the square bracket of equation 4.2 represents the current flowing from the semiconductor to the metal, which is governed by the concentration of electrons with enough energy to surmount the potential barrier of the space-charge region and cross the interface. Under forward bias, the concentration of such electrons increases. The second term of the square bracket represents the barrier to current flow in the opposite direction, which is insensitive to the applied bias. That reverse current is equal in magnitude to the forward current at zero-bias, when the net flow is zero. As can be seen from equation 4.3, the saturation current is governed by the barrier height, a function of the specific materials chosen.

Real Schottky contacts deviate from this behavior because of Fermi level pinning and surface dipoles. A sufficiently large density of surface-states can make the barrier

height insensitive to the metal work function, as the potential difference of the two phases is accommodated by the surface-states rather than the space-charge region. Surface dipoles, approximated by a perfect double-layer, introduce a discontinuity in potential, altering the effective electron affinity by an amount $\delta\chi = \sigma M/\varepsilon_0$, where σ is the surface density of the polar molecules that make up the layer, and M is their dipole moment.

4.1.2 Barrier Height Determination

The barrier height can be determined from equations 4.2 and 4.3. The Richardson constant and Schottky barrier lowering are voltage dependent, but can be incorporated into an ideality factor n, so that

$$J \sim \exp\left(-\frac{qV}{nkT}\right) \tag{4.4}$$

and n should be close to 1. The saturation current can then be found by extrapolating to zero bias, and the barrier height is found by rearranging equation 4.3 to

$$\phi_{Bn} = \frac{kT}{q} \ln\left(\frac{A^* T^2}{J_{ST}}\right) \tag{4.5}$$

Fortunately, the barrier height is not very sensitive to the precise value of the A^*, which may not be known.

The flat-band potential, and thus the barrier height, can be determined from the capacitance-voltage behavior. Assuming a uniform ionized dopant density up to the end of the depletion region, the charge Q per unit area A associated with the depletion

width W (defined in Chapter 1) can be written as

$$\frac{Q}{A} = qN_DW = \sqrt{2q\varepsilon\varepsilon_0 N_D \left(V_s - \frac{kT}{q}\right)} \tag{4.6}$$

where V_s is the surface potential, the difference between the band-edge positions in the bulk and at the surface. Differentiating the charge with respect to the surface potential yields

$$\frac{1}{A}\frac{\delta Q}{\delta V_s} = \frac{C}{A} = \sqrt{\frac{q\varepsilon\varepsilon_0 N_D}{2\left(V_s - \frac{kT}{q}\right)}} \tag{4.7}$$

The capacitance measured is the ratio of the change in charge at the surface to the change in voltage applied across the semiconductor, also called the differential capacitance. This is physically realized by modulating the surface potential with a small AC voltage applied in addition to the DC bias, V. Rearrangement of equation 4.7 and separation of V_s into its components V_{bi}, the built-in voltage, and V, the DC bias, gives[1]

$$\left(\frac{C_{sc}}{A}\right)^{-2} = \left(\frac{2\left(-V + V_{bi} + \frac{kT}{q}\right)}{q\varepsilon\varepsilon_0 N_D}\right) \tag{4.8}$$

V_{bi} is determined by plotting C^{-2} vs V and extrapolating to the voltage intercept, where $V = V_{bi} + \frac{kT}{q}$. Once V_{bi} is known, Φ is known because $\Phi = V_{bi} + V_n$ and V_n is determined from N_D.

The above treatment does not account for surface-states. The measured differential capacitance is the sum of the space charge region capacitance, C_{SC}, and the

surface-state capacitance, C_{SS}. The occupation statistics of the surface-states, and hence C_{SS}, are dependent upon the surface potential. C_{SS} is also dependent upon the capture and emission kinetics of the surface states. The change in observed capacitance due to carrier capture and emission by defect states can be useful for material characterization by techniques such as deep-level transient spectroscopy.[2] However, this will lead to non-linear deviations from the desired $C^{-2} - V$ relationship for the frequencies and surface potentials in which the surface-states are active.[3–5]

4.1.3 Mercury Soft Contacts

Mercury contacts provide a useful test system for probing the effects of surface modification upon diode formation. The high surface tension of the metal allows the contact to avoid being dominated by physically recessed defects such as pinholes. Importantly, the contact is formed at room temperature, so unwanted chemical reactions that often occur during contact formation are avoided.[6–8]

Mercury has been especially useful for testing silicon surfaces because the 4.49 eV work function would ideally put contacted Si of either dopant type into rectifying depletion conditions. Ge has a very similar electron affinity to silicon, so n-type Ge would be expected to form rectifying Hg contacts, but the valence band position is very close to the Hg work function and p-Ge would not be expected to form clearly rectifying contacts.

Synchrotron experiments performed on CH_3-Si(111) and H-Si(111) show the effective electron affinity (χ_{eff}) deviates significantly from the bulk affinity of 4.05 eV

to values of 3.67 eV and 4.17 eV, respectively.[9] These shifts were confirmed with Hg/Si contacts, where n-type CH_3-Si(111) and p-type H-Si(111) were strongly rectifying but the n-type H-Si(111) and p-type CH_3-Si(111) were not.[8] Hg/Ge contacts have not been studied as thoroughly, but experiments conducted on Ge electrodes have demonstrated that alkane modified surfaces can allow rectifying contacts to be formed on n-type and intrinsic substrates.[10] The research presented here examines Hg contacts on CH_3-, C_2H_5-, and $C_{10}H_{21}$-Ge(111) surfaces. Unlike the field effect experiments of the previous chapter, the semiconductor surface is in thermal equilibrium with a conducting phase, so the surface energetics are affected by the surface dipole.

4.2   Experimental

Single-side polished samples with an area of approximately 1 cm^2 were alkylated as described in Chapter 2. Ga/In eutectic was spread across the rough surface to form an ohmic contact. The sample was placed rough side down on a copper plate and a Teflon tube was lowered to press an o-ring against the polished surface. Electronic grade mercury (Alfa Aesar) was poured into the Teflon barrel to contact the area of the sample surface within the o-ring. A platinum wire was immersed into the top of the mercury column to allow electrical connection. Connections were made to a 1286 Solartron Potentiostat and Schlumberger SI 1260 Frequency Response Analyzer in a two-electrode configuration with the copper plate as the working electrode and the platinum wire as the counter electrode. The area of the mercury contact was verified by contacting the mercury column to a gold-coated glass slide and measuring

98

Figure 4.1: Equivalent circuit

the resulting hole in the gold layer.

$I-V$ curves were measured in the range -0.4 to 0.6 V, or up to 200 mA. Impedance analysis was performed under reverse bias conditions (0–0.6 V) with 10 mV AC modulation. The AC frequency was varied from 10^2–10^6 Hz. Curve fitting of the Bode and Nyquist plots to the model circuit in Figure 4.1 was accomplished with the Z-plot package.

4.3   Results

Results for methyl-, ethyl-, and decyl-terminated surfaces of on substrates of different dopant density (denoted **I-V**) are collected in Table 4.1. Wafer **I** was undoped, wafers **II-V** were antimony doped. Junctions that could not be fitted to the simple cell in Figure 4.1, for example requiring replacement of the parallel capacitance with a constant phase element, are not included, with the exception of those from wafer **I** because no undoped samples were obtained that showed the desired behavior. P-type samples, oxidized samples, and samples prepared by thermal hydrogermylation with 1-decene did not show rectification necessary to calculate a barrier height. Figure 4.2 shows J-V curves of three Hg/Ge(111) Schottky junctions. The solid line is from a $C_{10}H_{21}$-Ge(111) surface derived from modification of an n-type substrate with decylmagnesium bromide. The dot-dashed curve is from a CH_3-Ge(111) surface,

derived from the modification of an undoped substrate (wafer **I**) with methylmagnesium bromide. The dashed curve is of $C_{10}H_{21}$-Ge(111) surface derived from the thermal hydrogermylation reaction with H-Ge(111). The dashed curve showed very little rectification, so no differential capacitance date could be collected.

The sample represented by the solid line of Figure 4.2 showed a greater degree of rectification, and more ideal behavior, as displayed in Figures 4.3 and 4.4. The impedance increased linearly with a slope of 1, over a frequency range of almost two decades, and the phase angle of the AC current approached $90°$, indicating the parallel capacitance of the space-charge region dominated the system impedance over those frequencies. The differential capacitance values obtained by fitting the frequency response data to the circuit in Figure 4.1 were used to construct the Mott-Schottky plots in Figure 4.5. The CH_3-Ge(111) and $C_{10}H_{21}$-Ge(111) samples were from the same wafer and ideally would have had the same slope. Such variations, possibly due to differences in contact area, are reflected in the dopant density values in Table 4.1.

The undoped samples, represented by the center curve of Figure 4.2, displayed rectification, but as can be seen from Figures 4.6, 4.7, and 4.8, a single capacitance was not the dominant element over any frequency range, so the equivalent circuit was not a useful model and a straightforward Mott-Schottky analysis was not possible.

Table 4.1: Junction Properties of Hg/Ge(111)

sample type	$C^{-2} - V$ measurements		$J - V$ measurements	
	$N_\mathrm{D}(\mathrm{cm^{-3}})^a$	$\Phi_{\mathrm{Bn},C^{-2}-V}(\mathrm{V})$	quality factor n	$\Phi_{\mathrm{Bn},J-V}(\mathrm{V})$
CH$_3$-Ge **I**	N/A^b	N/A^b	2.0 ± 0.2	0.53 ± 0.05
C$_{10}$H$_{21}$-Ge **I**	N/A^b	N/A^b	2.15 ± 0.08	0.52 ± 0.01
CH$_3$-Ge **II**	$1.3 \pm 0.2 \times 10^{15}$	0.44 ± 0.12	1.6 ± 0.2	0.55 ± 0.05
C$_2$H$_5$-Ge **II**	$3.6 \pm 0.4 \times 10^{14}$	0.67 ± 0.07	1.6 ± 0.2	0.55 ± 0.05
C$_{10}$H$_{21}$-Ge **II**	$3.7 \pm 0.4 \times 10^{14}$	0.56 ± 0.06	1.68 ± 0.2	0.57 ± 0.05
CH$_3$-Ge **III**	$7.9 \pm 0.3 \times 10^{16}$	0.43 ± 0.03	1.45 ± 0.28	0.65 ± 0.03
C$_2$H$_5$-Ge **III**	$7.9 \pm 1 \times 10^{16}$	0.61 ± 0.09	1.07 ± 0.02	0.67 ± 0.02
C$_{10}$H$_{21}$-Ge **III**	$4.6 \pm 0.4 \times 10^{16}$	0.63 ± 0.05	1.21 ± 0.04	0.61 ± 0.01
CH$_3$-Ge **IV**	$6.7 \pm 0.6 \times 10^{15}$	0.52 ± 0.07	1.34 ± 0.11	0.60 ± 0.03
C$_{10}$H$_{21}$-Ge **IV**	$4.2 \pm 0.5 \times 10^{15}$	0.61 ± 0.04	1.15 ± 0.05	0.69 ± 0.01
CH$_3$-Ge **V**	$1.1 \pm 0.4 \times 10^{17}$	0.47 ± 0.1	1.6 ± 0.2	0.65 ± 0.05
C$_{10}$H$_{21}$-Ge **V**	$0.9 \pm 0.4 \times 10^{17}$	0.8 ± 0.2	1.4 ± 0.3	0.63 ± 0.05

a Donor density as determined by the slope. *b* Not available, data could not be fit to equivalent circuit model in Figure 4.1.

Figure 4.2: Representative *J-V* curves of alkylated Ge(111)/Hg Schottky contacts. Solid line is for n-type Ge(111) surface derived from decylmagnesium bromide, dashed line is undoped Ge(111) surface derived from methylmagnesium bromide, dotted line is from n-type Ge(111) derived from 1-decene.
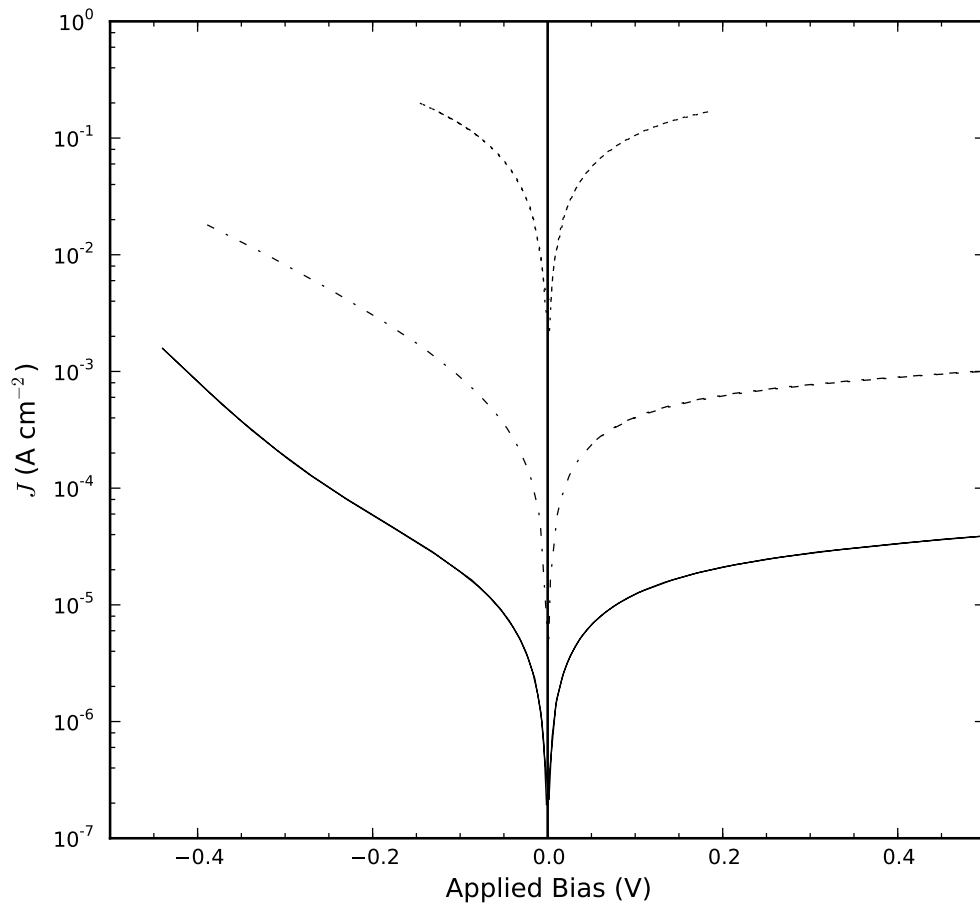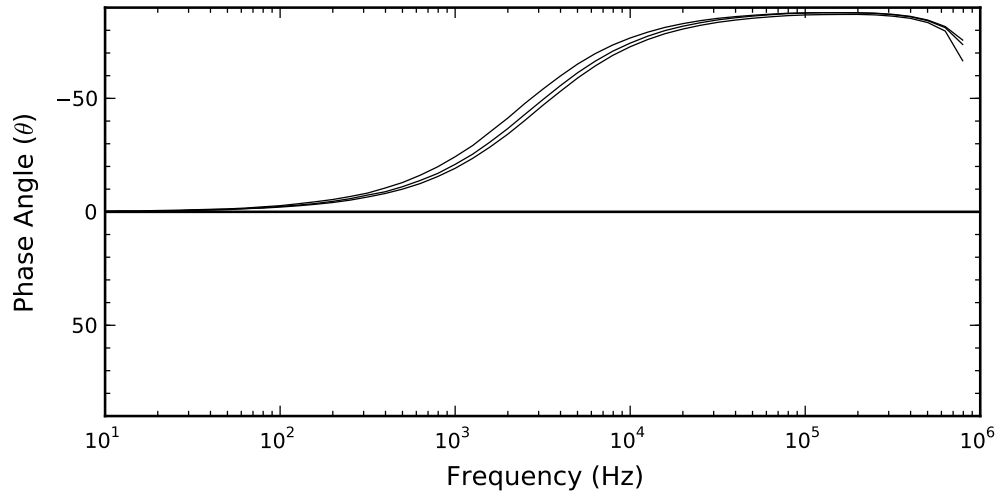
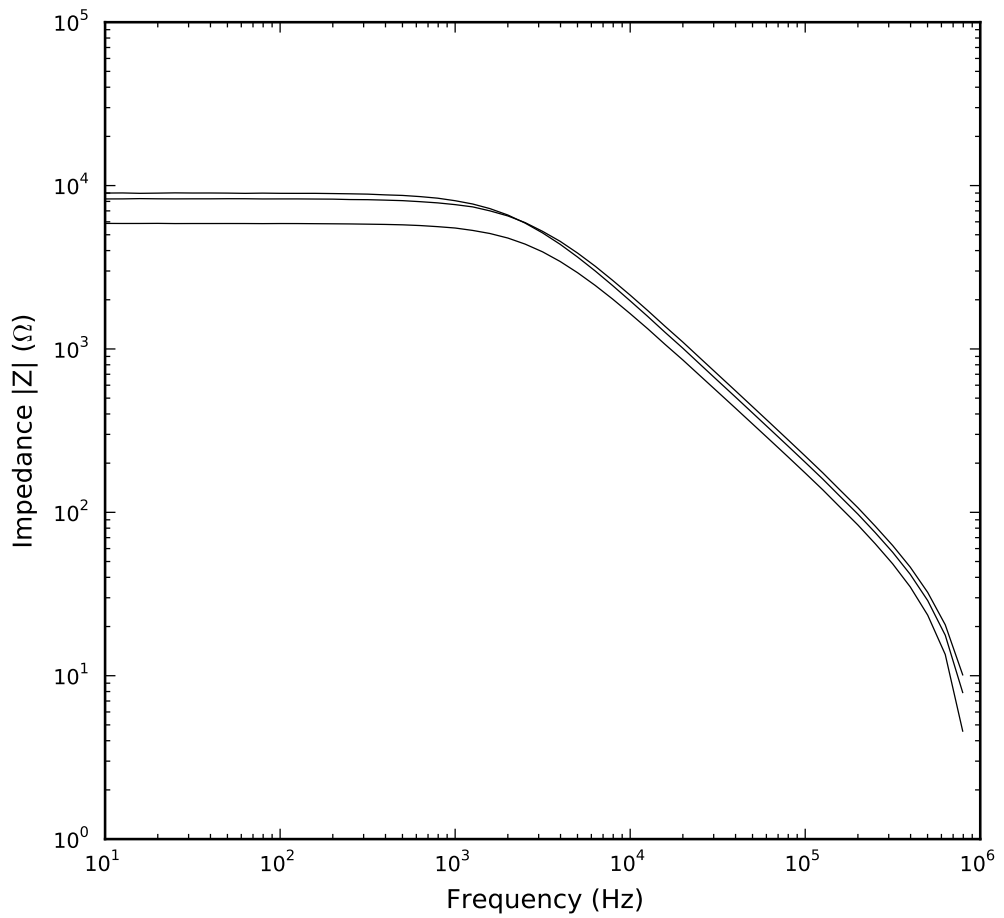Figure 4.3: Hg/$C_{10}H_{21}$-Ge(111) junction (wafer **III**)

(a)

(b)

Figure 4.4: Hg/CH$_3$-Ge(111) junction (wafer **III**)

(a)
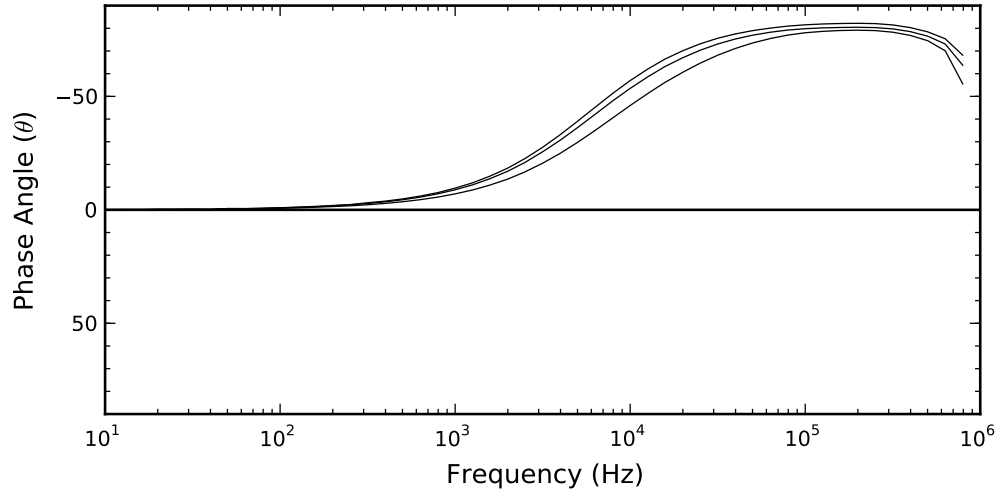
(b)
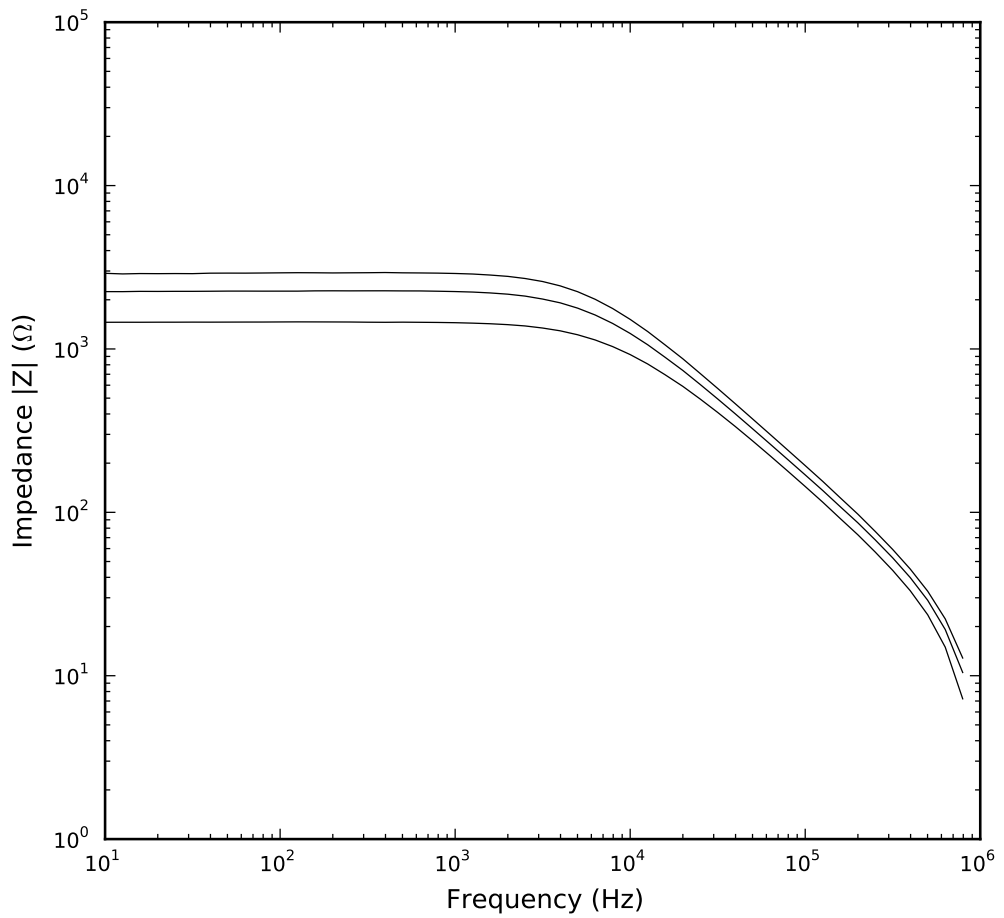
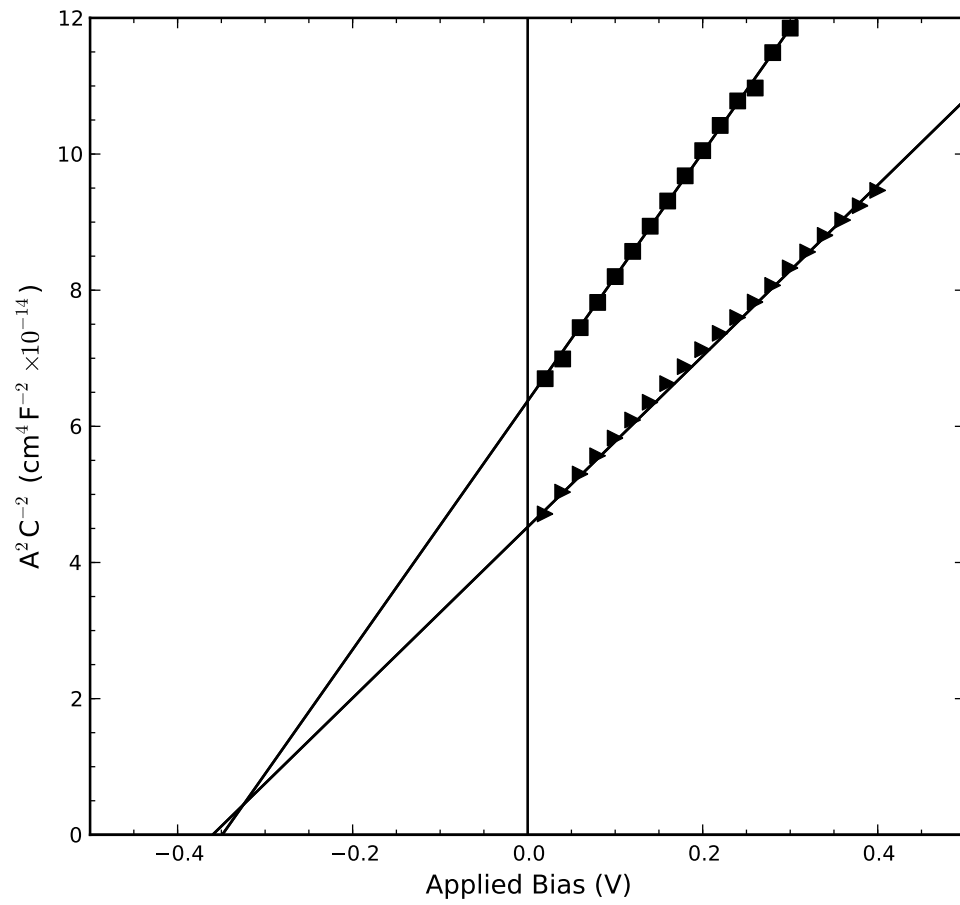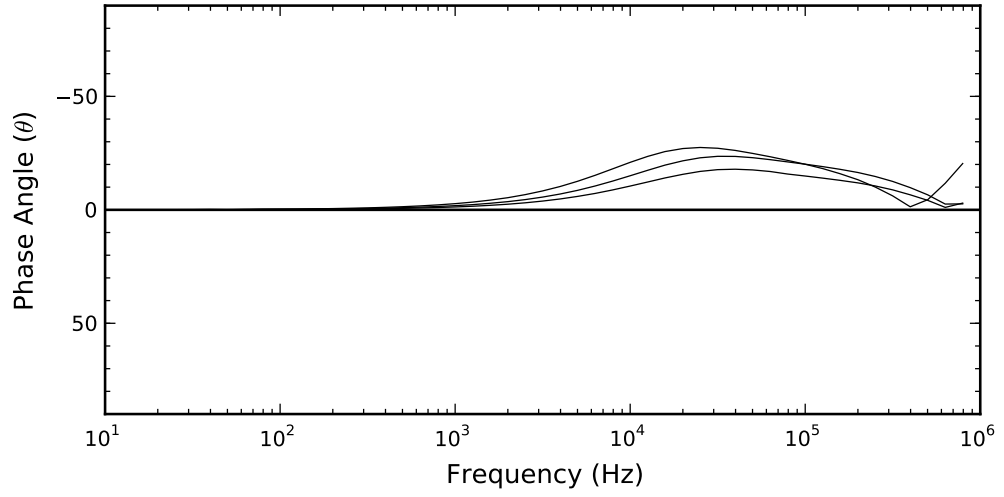Figure 4.5: Mott-Schottky plots for Hg/CH$_3$- and C$_{10}$H$_{21}$-Ge(111) junction (wafer **III**)

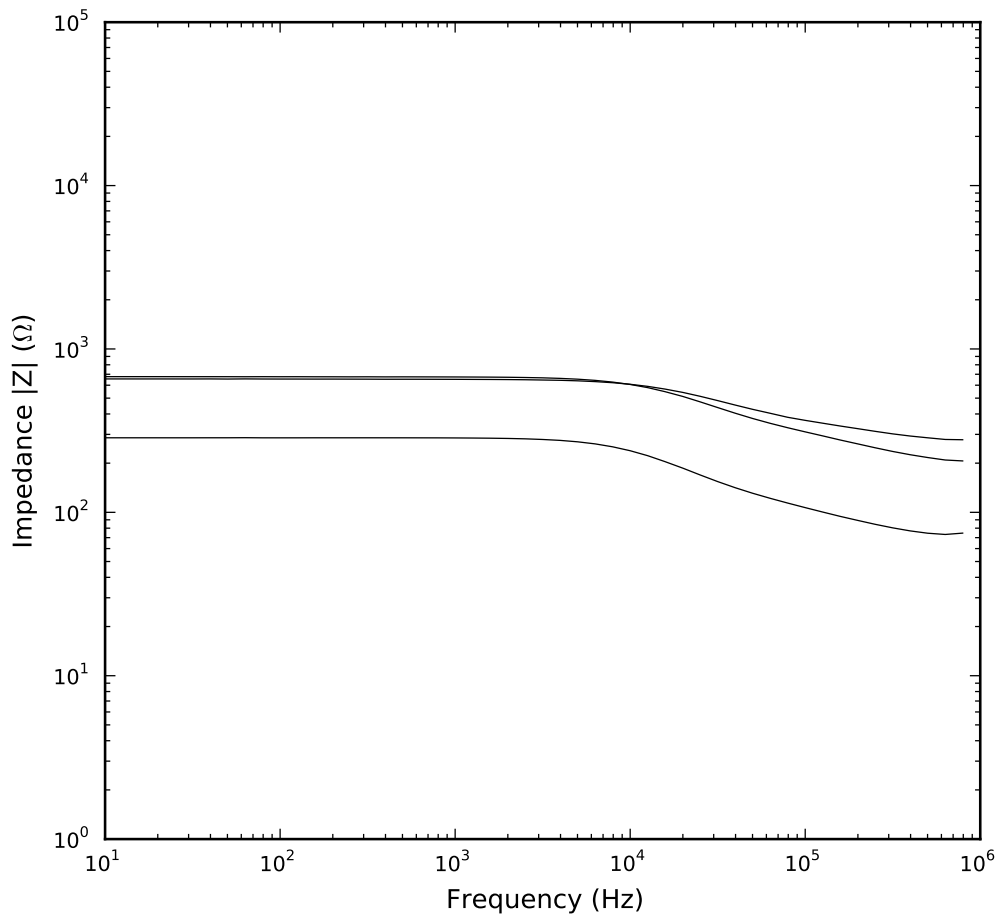Figure 4.6: Hg/C$_{10}$H$_{21}$-Ge(111) junctions (wafer **I**)
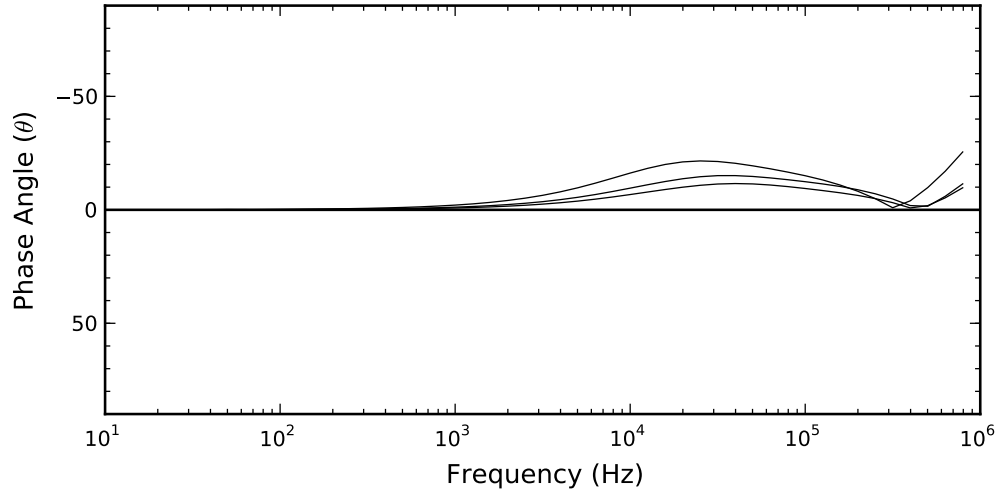
(a)

(b)

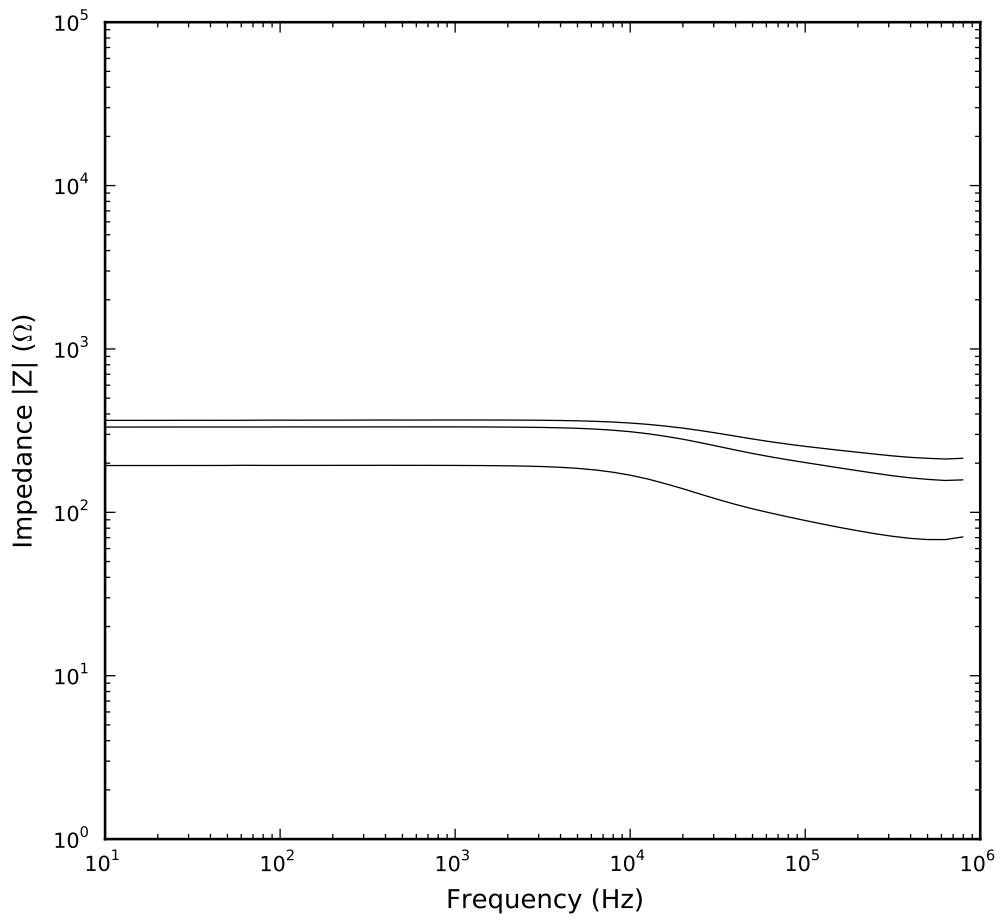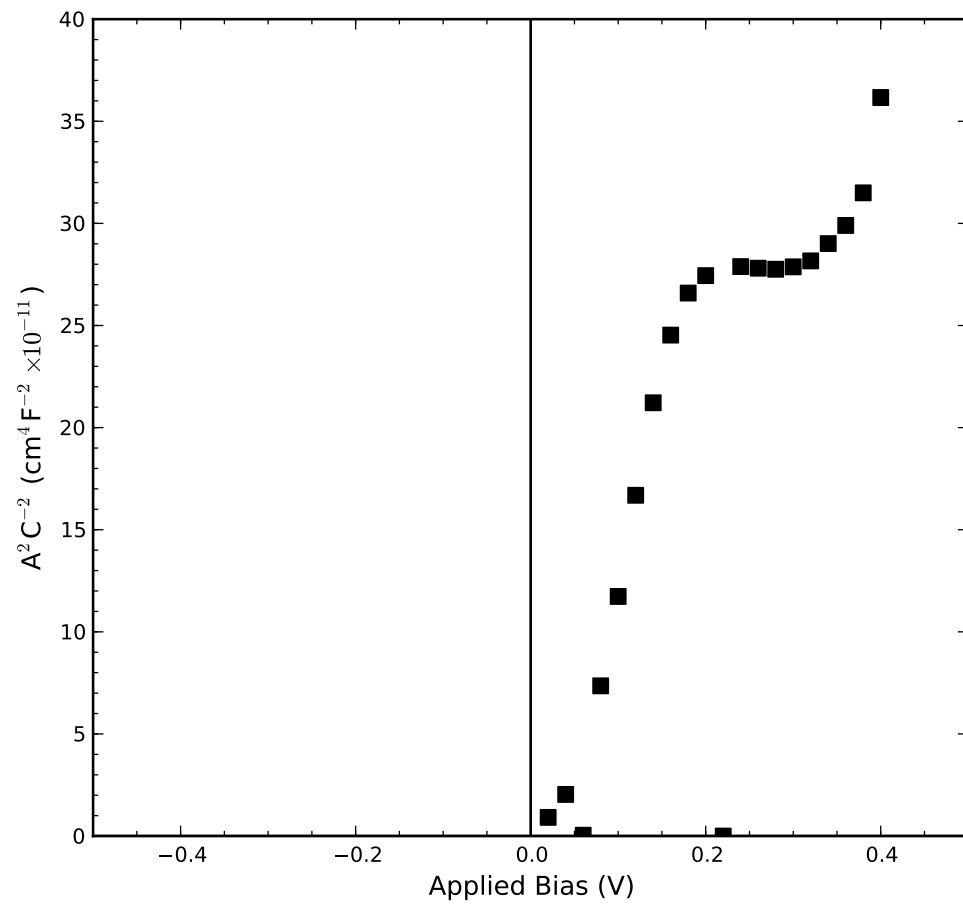Figure 4.7: Hg/CH$_3$-Ge(111) junctions (wafer **I**)

(a)

(b)

Figure 4.8: Mott-Schottky plots for Hg/CH$_3$-Ge(111) junction (wafer **I**)

4.4 Discussion

Of the samples studied, rectifying contacts with sufficient uniformity to allow flat-band measurements could only be formed with those prepared through the halogenation/alkylation method. This is in agreement with the conductance data of Chapter 3, which indicated all other surfaces were under n-type accumulation conditions. Sharp et al. were able to measure rectifying contacts with surfaces treated with 1-octadecene, and reported a barrier height of 0.41 V for n-type Ge(100) samples.[10] The contacts were not ideal however, because the reported ideality factors were greater than 2, indicating deviations from the thermionic emission process. A significant shift in barrier height due to a surface dipole would not be expected for a (100) surface because the arrangement and density of surface bonds do not allow as high a density of alkane moieties with the necessary orientation.[11] Hydrocarbon moieties with two or more carbons do not result in as high a surface dipole as do methyl groups.[12] Therefore, a lower barrier height for large alkanes on a (100) surface, relative to that seen on the (111) surface, could be expected if surface dipoles influenced the conditions at the junction.

Within error, the barrier heights from $C^{-2} - V$ and $J - V$ data were in agreement with a barrier height of 0.6 V, over 100 mV higher than predicted simply from the bulk electron affinity and Hg work function. This is smaller than the approximately 400 mV shift in the χ_{eff} of CH_3-Si(111) seen in photoelectron measurements and Hg junctions.[8,9] Because the electronegativity of Ge is very similar to that of Si (2.01 versus 1.90), the surface atomic density is similar (7.84×10^{14} (Si) vs 7×10^{14}(Ge)),

and the C-H bonds have the same orientation, the dipole responsible for the shift should be similar. However, the bandgap of Ge is only 0.67 eV, so the possible barrier height is limited and differences in surface dipoles cannot be determined from the measured Hg/n-Ge(111) junction barrier heights.

The lack of rectification for Hg contacts to p-type substrates is consistent with the high barrier heights that were observed for n-type Ge(111) samples treated with the halogenation/alkylation procedure. While the measured Hg/n-Ge(111) barrier heights do not distinguish between ideal behavior or the pinning traditionally seen in solid-state Schottky contacts to n-Ge, they do confirm the lack of pinning at a positive surface potential associated with a surface oxide.

4.5   Conclusion

N-type Ge(111) surfaces modified through the halogenation/alkylation process exhibited barrier heights of 0.6 ± 0.1 V. The differential capacitance versus voltage behavior of such junctions indicated near-ideal behavior, in contrast to substrates that were either left unprotected or modified with 1-decene, which showed little detectable rectification. Differences in barrier height due to Fermi level pinning or due to surface dipole effects of methyl groups versus ethyl or decyl groups could not be resolved because of the narrow bandgap of Ge and the instability of H-Ge(111).

Bibliography

[1] Sze, S. *Physics of Semiconductor Devices*, 2nd ed.; John Wiley & Sons: New York, 1981.

[2] Lang, D. *J. Appl. Phys.* **1974**, *45*, 3023–3032.

[3] Dewald, J. *Bell Syst. Tech. J.* **1960**, *39*, 615.

[4] Hens, Z.; Gomes, W. *Phys. Chem. Chem. Phys.* **1999**, *1*, 3607–3615.

[5] Huygens, I.; Strubbe, K. *J. Electrochem. Soc.* **2008**, *144*, F49–F54.

[6] Choi, J.; Ahmed, S.; Dimitrova, T.; Chen, J.; Schroder, D. *IEEE Trans. Electron Dev.* **2004**, *51*, 1380–1384.

[7] Hunger, R.; Fritsche, R.; Jaeckel, B.; Webb, L.; Jaegermann, W.; Lewis, N. *Surf. Sci.* **2007**, *601*, 2896–2907.

[8] Maldonado, S.; Plass, K.; Knapp, D.; Lewis, N. *J. Phys. Chem. C* **2007**, *111*, 17690–17699.

[9] Hunger, R.; Fritsche, R.; Jaeckel, B.; Jaegermann, W.; Webb, L.; Lewis, N. *Phys. Rev. B* **2005**, *72*, 045317.

[10] Sharp, I.; Schoell, S.; Hoeb, M.; Brandt, M.; Stutzmann, M. *Appl. Phys. Lett.* **2008**, *92*, 223306.

[11] Zandvlient, H. *Phys. Rep.* **2003**, *388*, 1–40.

[12] Jaeckel, B.; Hunger, R.; Webb, L.; Jaegermann, W.; Lewis, N. *J. Phys. Chem. C* **2007**, *111*, 18204–18213.